

Electronic structure of ultralong-range Rydberg penta-atomic molecules with two polar diatomic molecules

Javier Aguilera-Fernández,¹ H. R. Sadeghpour,² Peter Schmelcher,^{3,4} and Rosario González-Férez¹

¹*Instituto Carlos I de Física Teórica y Computacional, and Departamento de Física Atómica, Molecular y Nuclear, Universidad de Granada, 18071 Granada, Spain*

²*ITAMP, Harvard-Smithsonian Center for Astrophysics, Cambridge, Massachusetts 02138, USA*

³*The Hamburg Center for Ultrafast Imaging, Luruper Chaussee 149, 22761 Hamburg, Germany*

⁴*Zentrum für Optische Quantentechnologien, Universität Hamburg, Luruper Chaussee 149, 22761 Hamburg, Germany*

(Received 2 October 2017; published 28 November 2017)

We explore the electronic structure of ultralong-range penta-atomic Rydberg molecules from a merger of a Rydberg atom and two ground-state heteronuclear diatomic molecules. Our focus is on the interaction of Rb(23s) and Rb($n = 20$, $l \geq 3$) Rydberg states with ground and rotationally excited KRb diatomic polar molecules. For symmetric and asymmetric configurations of the penta-atomic Rydberg molecule, we investigate the metamorphosis of the Born-Oppenheimer potential curves, essential for the binding of the molecule, with varying distance from the Rydberg core and analyze the alignment and orientation of the polar diatomic molecules.

DOI: [10.1103/PhysRevA.96.052509](https://doi.org/10.1103/PhysRevA.96.052509)

I. INTRODUCTION

Recent experimental advances in ultracold physics allow for the creation of hybrid quantum systems formed by mixtures of atoms and atomic ions [1,2], atoms and molecules [3] or molecular ions [4,5], or by Rydberg-atom-based mixtures [6,7]. The study of these hybrid systems is motivated by a broad range of perspectives and potential applications, including precision measurements, ultracold chemistry [8], ultracold collisions [9], and quantum technologies [10]. These systems also provide a unique platform to investigate fundamental questions in few- and many-body quantum physics.

In an ultracold atomic cloud, a hybrid system consisting of a ground state and a Rydberg atom has theoretically been predicted to form an ultralong-range molecule [11]. The binding mechanism of this exotic Rydberg molecule is based on the low-energy collisions between the Rydberg electron and the ground-state atom [12,13]. These ultralong-range Rydberg molecules were first experimentally observed for Rb atoms in a s -wave Rydberg state [14], and current experiments focus on exploring these Rydberg molecules formed by higher angular momentum Rydberg states [15–20] and by other atomic species such as Cs [18,19] and Sr [21,22]. In a mixture of ultracold atoms and ultracold molecules, Rydberg atoms could be created by standard two-photon excitation schemes. In such a hybrid system, exotic giant polyatomic Rydberg molecules are predicted to exist if a heteronuclear diatomic molecule, either a Λ -doublet or a rotating polar molecule, is immersed into the Rydberg wave function [23–26]. The binding mechanism appears due to anisotropic scattering of the Rydberg electron from the permanent electric dipole moment of the polar molecule. This coupling gives rise to a mixing between the two opposite-parity internal states of a Λ -doublet molecule or rotational states of a rigid rotor [23,26]. It should be noted that heteronuclear diatomic molecules with subcritical permanent electric dipole moment ($d < 1.639$ D) are preferred to prevent binding of the Rydberg electron to the polar molecule [27–30].

The electronic structure of these giant Rydberg molecules possesses oscillating Born-Oppenheimer potentials (BOP)

with well depths of either a few GHz or a few MHz if they evolve from the Rydberg degenerate manifold with orbital quantum number $l > 2$ [23–26] or from the Rydberg states with lower orbital angular momentum $l \leq 2$ [31], respectively. The Rydberg-electron-induced coupling gives rise to a strong hybridization of the rotational states and a strong orientation and alignment of the diatomic molecule. Since in the giant Rydberg molecule, the orientation of the diatomic molecule changes sign as the distance from the Rydberg core varies [23,26], two internal rotational states of opposite orientation could be Raman coupled [23] to create a switchable dipole-dipole interaction needed to implement molecular qubits [32]. A nondestructive scheme to readout the internal state of polar molecules has been proposed based on the Rydberg-field-induced interaction with the molecular electric dipole moment [33,34].

In such an ultracold mixture of Rydberg atoms and molecules, it can occur, for sufficiently dense gases, that more than one diatomic molecule might immerse in the Rydberg orbit, creating the possibility of more complex polyatomic Rydberg molecules. In the present work, we consider a penta-atomic molecule (PentaMol) formed by a Rydberg atom and two ground-state heteronuclear diatomic molecules. As in our previous study on the triatomic Rydberg molecule [26], we include the angular degrees of freedom of the diatomic molecules within the rigid rotor approximation. This treatment of the internal motion of the diatomic molecules allows us to properly investigate the effect of the electric fields due to the Rydberg core and electron on their directional properties.

Our focus is on two collinear configurations of two polar diatomic molecules bound within the Rydberg orbit—a symmetric one in which the two diatomic molecules are located at different sides of the Rydberg core, see Fig. 1(a), and an asymmetric one where they are on the same side as shown in Fig. 1(b). As prototype ultralong-range molecules, we consider those formed by the rubidium Rydberg atom and the diatomic molecules KRb. The rotational constant of KRb is $B = 1.114$ GHz [35] and its electric dipole moment $d = 0.566$ D [36], which is well below the Fermi-Teller critical value

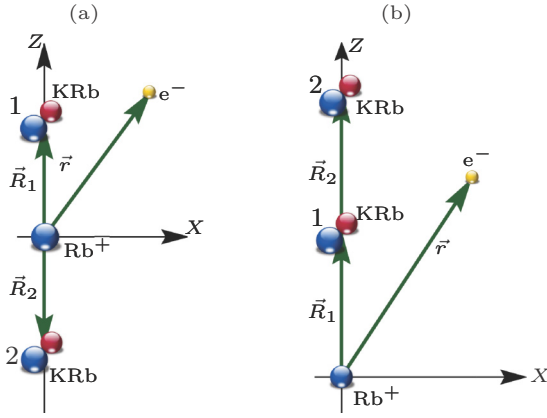


FIG. 1. A sketch (not to scale) of the Rydberg PentaMol formed by a Rydberg atom and two diatomic polar molecules in the (a) symmetric and (b) asymmetric configurations. The first and second diatomic molecules, as referred to throughout the text, are identified in these sketches with 1 and 2, respectively.

1.639 D [27,28]. We analyze the adiabatic electronic potentials of the symmetric configurations KRb-Rb($n = 20, l \geq 3$)-KRb and KRb-Rb($23s$)-KRb Rydberg PentaMols, as the separation between the two KRb molecules and the Rb⁺ core varies. We equally explore the effects of the electric field due to the Rydberg atom on the rotational motion of diatomic molecules by analyzing their orientation and alignment. For the asymmetric configuration, we study the BOPs of Rb($n = 20, l \geq 3$)-KRb-KRb as the distance of one or two of the diatomic molecules from the Rydberg core increases. For the adiabatic electronic states, we encounter oscillating BOPs having potential wells with depths from a few MHz to a few GHz, depending on the Rydberg state of Rb involved in the giant Rydberg PentaMol.

The adiabatic Hamiltonian of the Rydberg molecule is introduced in Sec. II, where we also provide the coupled basis used to solve the underlying Schrödinger equation. In Sec. III we analyze the electronic structure of the linear symmetric and asymmetric configurations as the distance of the diatomic molecules from the Rydberg core increases, and analyze their directional properties. The conclusions are provided in Sec. IV. The expression of the electric field due to the Rydberg electron is provided in the Appendix.

II. THE ADIABATIC HAMILTONIAN

We consider a polyatomic molecule formed by a Rydberg atom and two ground-state heteronuclear diatomic molecules. The ground-state diatomic molecules are described within the Born-Oppenheimer and rigid rotor approximations, i.e., we adiabatically separate first the electronic and nuclei degrees of freedom, and then the vibrational and rotational motions. These approximations provide a good description of deeply bound diatomic molecules in the presence of moderate electric fields [37,38]. The electric field due to the Rydberg electron and the ion at position \mathbf{R}_i is

$$\mathbf{F}_{\text{Ryd}}(\mathbf{R}_i, \mathbf{r}) = e \frac{\mathbf{R}_i}{R^3} + e \frac{\mathbf{r} - \mathbf{R}_i}{|\mathbf{r} - \mathbf{R}_i|^3}, \quad (1)$$

where e is the electron charge, \mathbf{r} is the position of the Rydberg electron, and $\mathbf{R}_i = \mathbf{R}_1, \mathbf{R}_2$ are the positions of the diatomic molecules. The full expression for the Rydberg electron's electric field is provided in the Appendix.

In the framework of the Born-Oppenheimer approximation, the adiabatic Hamiltonian of this Rydberg PentaMol is given by

$$H_{\text{ad}} = H_A + H_{\text{mol}}, \quad (2)$$

where H_A represents the single-electron Hamiltonian describing the Rydberg atom

$$H_A = -\frac{\hbar^2}{2m_e} \nabla_r^2 + V_l(r), \quad (3)$$

where $V_l(r)$ is the l -dependent model potential [39], with l being the angular momentum quantum number of the Rydberg electron.

The molecular Hamiltonian which describes the two diatomic molecules in the rigid-rotor approximation, the charge-dipole interaction, and the dipole-dipole interaction reads

$$H_{\text{mol}} = \sum_{i=1,2} [B\mathbf{N}_i^2 - \mathbf{d}_i \cdot \mathbf{F}_{\text{Ryd}}(\mathbf{R}_i, \mathbf{r})] + V_{12}(\Omega_1, \Omega_2), \quad (4)$$

with B being the rotational constant, \mathbf{N}_1 and \mathbf{N}_2 the molecular angular momentum operators, and \mathbf{d}_1 and \mathbf{d}_2 the permanent electric dipole moments of the diatomic molecules. Note that for a linear molecule, the electric dipole moment is parallel to the molecular internuclear axis. The last term $V_{12}(\Omega_1, \Omega_2)$ stands for the dipole-dipole interaction between the two diatomic molecules. For the Rydberg PentaMols considered in this work, the distance between the two diatomic molecules is large enough so that the dipole-dipole interaction could be neglected. For each diatomic molecule, the internal rotational motion is described by the Euler angles $\Omega_i = (\theta_i, \phi_i)$ with $i = 1, 2$.

The total angular momentum of the Rydberg molecule, excluding an overall rotation, is given by $\mathbf{J} = \mathbf{l} + \mathbf{N}$, where \mathbf{l} is the orbital angular momentum of the Rydberg electron, and \mathbf{N} is the total molecular angular momentum of the two diatomic molecules, $\mathbf{N} = \mathbf{N}_1 + \mathbf{N}_2$. To solve the Schrödinger equation associated with the Hamiltonian (2), we perform a basis set expansion in terms of the coupled basis

$$\begin{aligned} \Psi_{nlm, N}^{JM_J}(\mathbf{r}, \Omega_1, \Omega_2) &= \sum_{m_l=-l}^{m_l=l} \sum_{M_N=-N}^{M_N=N} \langle lm_l N M_N | J M_J \rangle \\ &\times \Psi_{N_1 N_2}^{N M_N}(\Omega_1, \Omega_2) \psi_{nlm}(\mathbf{r}), \end{aligned} \quad (5)$$

where $\langle lm_l N M_N | J M_J \rangle$ is the Clebsch-Gordan coefficient, $J = |l - N|, \dots, l + N$, and $M_J = -J, \dots, J$. $\psi_{nlm}(\mathbf{r})$ is the Rydberg electron wave function, with n , l , and m being the principal, orbital, and magnetic quantum numbers, respectively. For the two ground-state molecules, we use the coupled basis

$$\begin{aligned} \Psi_{N_1 N_2}^{N M_N}(\Omega_1, \Omega_2) &= \sum_{M_{N_1}=-N_1}^{M_{N_1}=N_1} \sum_{M_{N_2}=-N_2}^{M_{N_2}=N_2} Y_{N_1 M_{N_1}}(\Omega_1) \\ &\times Y_{N_2 M_{N_2}}(\Omega_2) \langle N_1 M_{N_1} N_2 M_{N_2} | N M_N \rangle, \end{aligned} \quad (6)$$

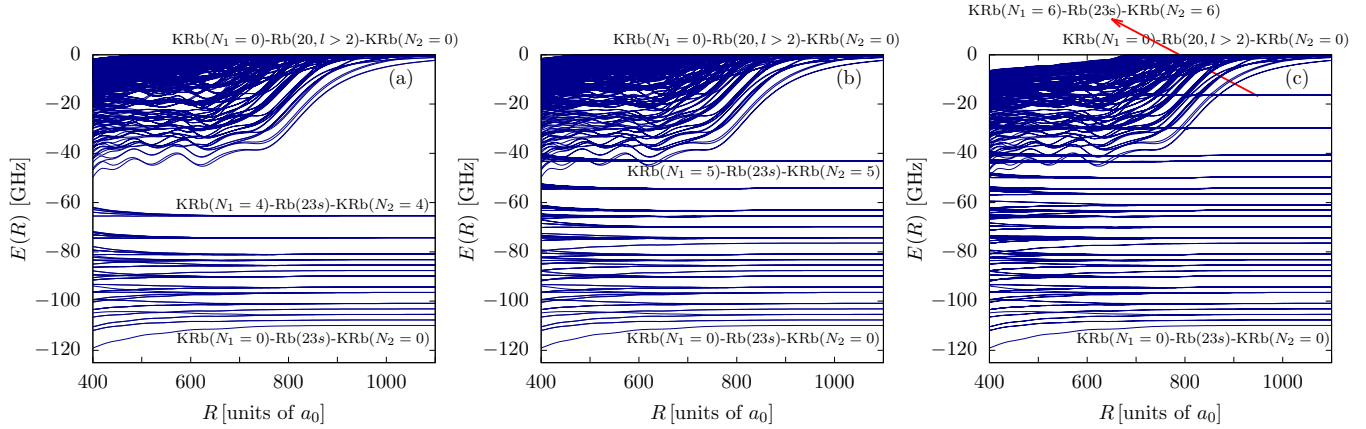


FIG. 2. Symmetric configuration of the Rydberg PentaMol: adiabatic electronic potential curves evolving from the degenerate manifold $\text{Rb}(n = 20, l \geq 3)$ and the Rydberg state $\text{Rb}(23s)$ for total magnetic quantum number $M_J = 0$. Calculations have been performed, including in the coupled basis of the diatomic molecule (6) rotational excitations up to (a) $N_i = 4$, (b) $N_i = 5$, and (c) $N_i = 6$, $i = 1, 2$.

where N_i and M_{N_i} , with $i = 1, 2$, are the rotational and magnetic quantum numbers, and $Y_{N_i M_{N_i}}(\Omega_i)$ is the field-free rotational wave function of the diatomic molecules, i.e., the spherical harmonics. The coupled angular momentum of the two diatomic molecules satisfies $N = |N_1 - N_2|, \dots, N_1 + N_2$, and its projections on the laboratory fixed frame $M_N = -N, \dots, N$. Throughout the text, we use the notation $|N, M_N, N_1, N_2\rangle$ to identify the rotational states of the two diatomic molecules in the coupled basis Eq. (6). Note that due to the Rydberg-field-induced coupling, N , M_N , N_1 , and N_2 are not good quantum numbers.

For the linear configuration of the Rydberg PentaMol, the electric field couples functions of the coupled basis (5) having the same total magnetic quantum numbers M_J . As a consequence, the basis set expansion of the wave function is done in terms of functions of the coupled basis (5) with the fixed total magnetic quantum number M_J .

III. THE BORN-OPPENHEIMER ADIABATIC POTENTIAL CURVES

Let us now explore the adiabatic potential energy curves, more precisely relevant intersections of the underlying potential energy surfaces, of the electronic states for the linear Rydberg PentaMol: a symmetric configuration and two asymmetric ones, presented in Fig. 1. We have first performed an analysis of the convergence behavior of the adiabatic electronic states for the symmetric configuration of the Rydberg molecule KRb-Rb-KRb , i.e., $R = R_1 = R_2$. The coupled basis (5) includes the wave functions of the Rydberg degenerate manifold $\text{Rb}(n = 20, l \geq 3)$ and of the energetically closest Rydberg state $\text{Rb}(23s)$. Note that we are neglecting the quantum defect of the nf Rydberg state. For the diatomic molecules, we take into account the rotational excitations up to $N_i = 4, 5$, and 6 , $i = 1, 2$, in the coupled basis of the two diatomic molecules (6), with the coupled angular momentum for the two KRb molecules $N \leq 8$, $N \leq 9$, and $N \leq 10$, respectively. The corresponding BOPs of the symmetric configuration of the Rydberg PentaMol for $M_J = 0$ are presented in Fig. 2. The zero energy has been set to the energy of the $\text{Rb}(n = 20, l \geq 3)$ degenerate manifold and

the two KRb molecules are in their rotational ground state $N_1 = N_2 = 0$.

The main difference between these three spectra are the additional BOPs belonging to electronic states evolving from the excited rotational states of KRb with $N_i = 5$ and $N_i = 6$, $i = 1, 2$, which do not appear in Fig. 2(a). The BOPs evolving from the Rydberg state $\text{Rb}(23s)$ can be easily identified in the electronic spectrum as approximately horizontal lines on the scale of these figures. These BOPs also present an oscillatory behavior with potential wells from a few tens to a few hundreds of MHz, which are not appreciated on the scale of these figures and will be discussed later on. These electronic states approach the asymptotic limit $\Delta E_{23s} + N_1(N_1 + 1)B + N_2(N_2 + 1)B$ for large values of R , with $\Delta E_{23s} = E_{23s} - E_{20, l \geq 3}$, E_{23s} and $E_{20, l \geq 3}$ being the energies of $\text{Rb}(23s)$ and $\text{Rb}(n = 20, l \geq 3)$, respectively. In the energetical region of the electronic states evolving from the Rydberg manifold $\text{Rb}(n = 20, l \geq 3)$ $E(R) \gtrsim -50$ GHz, we encounter a few BOPs evolving from $\text{Rb}(23s)$ and the two KRb molecules in a excited rotational state with $N_i \geq 5$. Due to high rotational excitations of the diatomic molecules, the effect of the Rydberg electric field is significantly reduced, since the electric-field interaction has to compensate for the large rotational kinetic energies of each KRb , which are 33.4 GHz and 46.8 GHz for $N_i = 5$ and $N_i = 6$, respectively. In contrast, in the lowest-lying electronic states from the Rydberg degenerate manifold $\text{Rb}(n = 20, l \geq 3)$, the two diatomic molecules evolve from their rotational ground states with zero rotational kinetic energies.

The relative errors of the BOPs of the six lowest-lying states evolving from the Rydberg manifold $\text{Rb}(n = 20, l \geq 3)$ are less than 1% when the rotational excitations of KRb are increased from $N_i \leq 4$ to $N_i \leq 5$, and decrease further by further increasing the range of N_i . Since in these electronic states the KRb molecules were initially in their rotational ground states, these small relative errors indicate that the contribution of rotational states with $N_i \geq 5$ is not significant on the field-dressed ground state. A similar conclusion can be derived for the electronic states evolving from the Rydberg state $\text{Rb}(23s)$ and the two KRb molecules with $N_i \leq 3$, and the comparison between the BOP for $N_i \leq 5$ and $N_i \leq 6$ shows relative errors around 1%. Finally, if only the states within

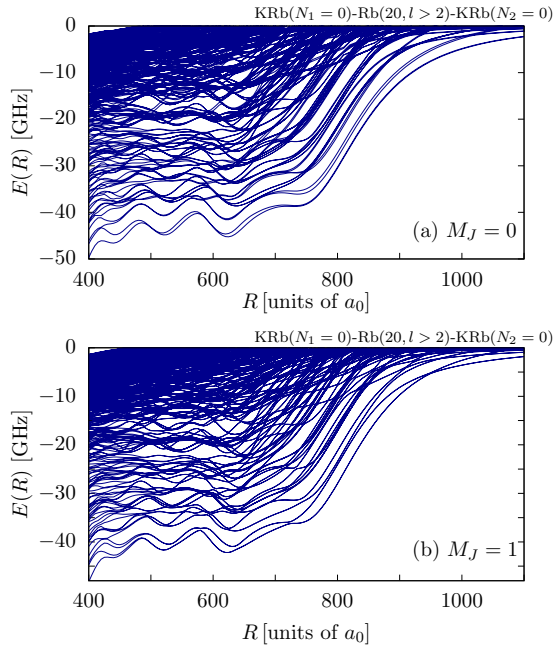


FIG. 3. Symmetric configuration of the Rydberg PentaMol: Adiabatic electronic potential curves evolving from the Rydberg manifold $\text{Rb}(n = 20, l \geq 3)$ with total magnetic quantum number (a) $M_J = 0$ and (b) $M_J = 1$.

the Rydberg degenerate manifold are included in the basis set expansion (excluding the nearby $23s$ state), the relative error is smaller than 0.8% for the six lowest-lying states. This is due to the large energy separation of 109.9 GHz between the Rydberg state $\text{Rb}(23s)$ and the manifold $\text{Rb}(n = 20, l \geq 3)$, and due to the fact that those electronic states evolving from $\text{Rb}(23s)$ and $\text{Rb}(n = 20, l \geq 3)$, which are energetically close, involve the KRb molecules in excited rotational states and in the ground state, respectively, which reduces their couplings.

A. The linear symmetric Rydberg molecule

In Figs. 3(a) and 3(b), we show the BOPs for $M_J = 0$ and 1, respectively, for the collinear Rydberg PentaMol where the two diatomic molecules are located on the Z axis of the laboratory fixed frame at the same distance from the core $R = R_1 = R_2$ but on different sides of Rb^+ , see the sketch presented in Fig. 1(a). For comparison, the corresponding adiabatic potentials for a Rb-KRb triatomic molecule (TriMol), with Rb^+ located at the center of the laboratory fixed frame and the diatomic molecule being on the Z axis at a distance $R = R_1$, are shown in Fig. 4. Note that the BOPs of the Rydberg TriMol also evolve from the $\text{Rb}(n = 20, l \geq 3)$ manifold. This Rydberg TriMol is numerically described with a coupled basis analogous to that used for the Rydberg PentaMol, see Ref. [26].

As for the Rydberg triatomic system, the electronic potentials oscillate as the distance between the diatomic molecules and Rb^+ $R = R_1 = R_2$ increases, which reflects the oscillatory behavior of the Rydberg electron wave function. These electronic states show many consecutive minima with depths of a few GHz, which accommodate vibrational bound states in which the Rydberg PentaMol is stable. We have

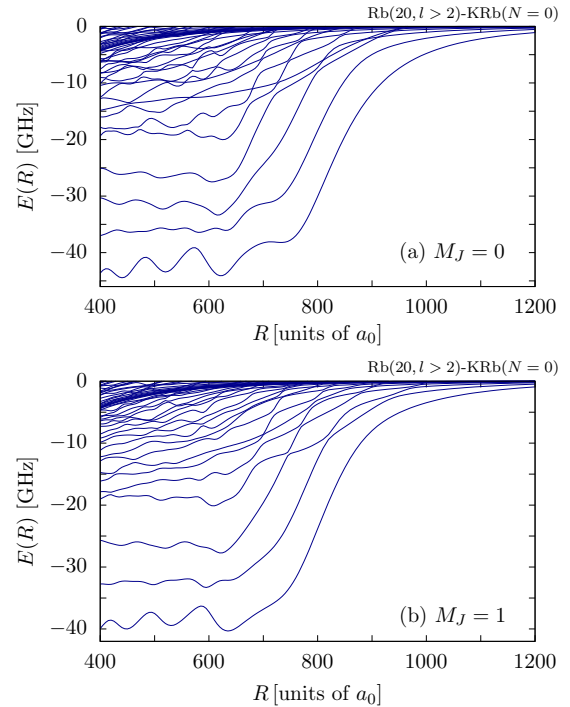


FIG. 4. Rydberg TriMol: Adiabatic electronic potential curves evolving from the Rydberg manifold $\text{Rb}(n = 20, l \geq 3)$ with total magnetic quantum number (a) $M_J = 0$ and (b) $M_J = 1$.

estimated that the outermost minima of the lowest-lying BOPs in Figs. 3(a) and 3(b) can accommodate six or seven vibrational bound states. The presence of the second diatomic molecule has two major effects on the electronic spectrum of the Rydberg PentaMol. First, there are more BOPs evolving from the Rydberg manifold $\text{Rb}(n = 20, l \geq 3)$; compare Fig. 3(a) with Fig. 4(a), and Fig. 3(b) with 4(b). This is due to the larger amount of possible rotational excitations of the two diatomic molecules, i.e., $\Psi_{N_1 N_2}^{N M_N}(\Omega_1, \Omega_2)$ with $N_i \leq 4$, to be combined with the Rydberg states from the degenerate manifold $\text{Rb}(n = 20, l \geq 3)$. As a consequence, the complexity of the electronic structure is significantly enhanced, and the neighboring electronic states undergo narrow avoided crossings. Second, the energy shifts of the two lowest-lying BOPs evolving from the Rydberg manifold $\text{Rb}(n = 20, l \geq 3)$ are somewhat larger compared to the corresponding shifts of the lowest-lying curves of the Rydberg TriMol in Fig. 4, but the differences are not significant. Indeed, for the Rydberg PentaMol, we also encounter pairs of electronic states possessing close energies, which at large separations once the effect of the electric field due to the Rydberg core becomes dominant, become degenerate. For $M_J = 1$, the degeneracy between pairs of consecutive states is manifest even at lower values of the separation R . The two KRb molecules are exposed to the internal Rydberg atom electric field, whose matrix elements within the Rydberg electron wave-function basis have the same strength but differ in sign due to their different locations on the Z axis (see Appendix). These two facts give rise to similar energetical shifts for the BOPs that are due to the presence of the first and second diatomic molecules, which are labeled in Fig. 1(a) with the numbers 1 and 2, respectively.

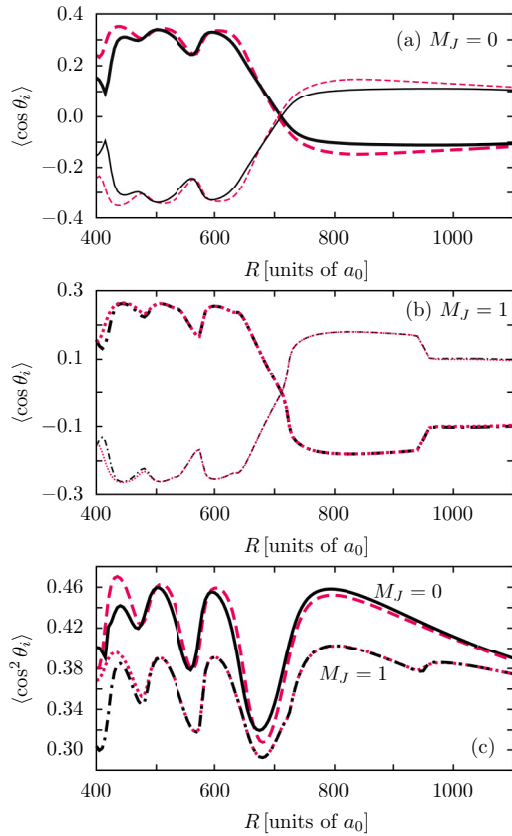


FIG. 5. Rydberg PentaMol: Orientation of the first (thin lines) and second (thick lines) diatomic molecule for the two lowest-lying adiabatic potentials evolving from the Rydberg manifold $\text{Rb}(n = 20, l \geq 3)$ for total magnetic quantum number (a) $M_J = 0$ and (b) $M_J = 1$. The alignment of these two diatomic molecules is identical and is presented for the two lowest-lying potentials for $M_J = 0$ and $M_J = 1$ in panel (c).

The KRB molecules within the Rydberg PentaMol are oriented and aligned due to the Rydberg electric field. Figures 5(a) and 5(b) present the orientation of the two diatomic molecules within the lowest-lying adiabatic electronic states from $\text{KRb-Rb}(n = 20, l \geq 3)\text{-KRb}$ for $M_J = 0$ and $M_J = 1$, respectively. The two KRB molecules are oriented in opposite directions but with the same absolute value, i.e., $|\langle \cos \theta_1 \rangle| = |\langle \cos \theta_2 \rangle|$. Within the BOPs for $M_J = 0$ and $R \lesssim 700 a_0$, the first diatomic molecule shows a moderate orientation off the Rydberg core whereas the second one is oriented towards Rb^+ . In both cases, their orientations show an oscillatory behavior reflecting the radial dependence of the Rydberg electron wave function. By further increasing the separation between Rb^+ and the KRB molecules, the value of the orientation for the two diatomic molecules is reversed. From there on, $|\langle \cos \theta_i \rangle|$, slowly approaches its zero field-free value. A similar behavior is observed for the orientation of the two KRB within BOPs for $M_J = 1$. For the orientation belonging to the $M_J = 1$ BOPs in Fig. 5(b), the sudden changes of the orientations at around $R \approx 950 a_0$ are due to an avoided crossing between these two potentials and the corresponding two neighboring ones according to Fig. 3(b). Within a certain electronic state, the alignment of the two diatomic molecules is the same,

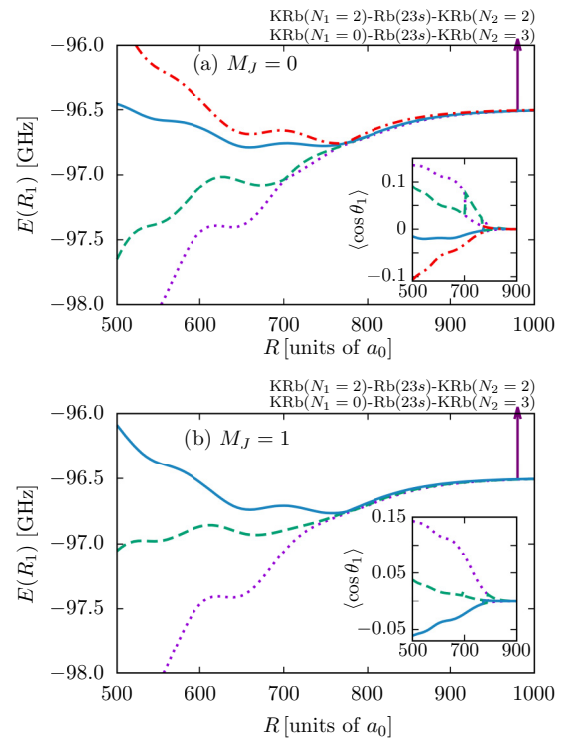


FIG. 6. Symmetric configuration of the Rydberg PentaMol: Adiabatic electronic potential curves with varying separation between the Rb^+ and the two diatomic molecules $R = R_1 = R_2$ evolving from the Rydberg state $\text{Rb}(23s)$ and for the diatomic molecules in rotational excitations with wave functions in the coupled basis $|N, M_N, 2, 2\rangle$, with $N = 0, \dots, 4$, $|3, M_N, 3, 0\rangle$, and $|3, M_N, 0, 3\rangle$. The total magnetic quantum number of the adiabatic electronic potentials is (a) $M_J = 0$ and (b) $M_J = 1$. The insets show the orientation of the first diatomic molecule $\langle \cos \theta_1 \rangle$ located at $\theta_1 = \phi_1 = 0$.

$\langle \cos^2 \theta_1 \rangle = \langle \cos^2 \theta_2 \rangle$; see Fig. 5(c) where we present $\langle \cos^2 \theta_i \rangle$ within these two lowest-lying BOPs for $M_J = 0$ and $M_J = 1$. The change of the direction of the orientation, i.e., $\langle \cos \theta_i \rangle \approx 0$, corresponds to the diatomic molecules having their field-free alignment $\langle \cos^2 \theta_i \rangle \approx 1/3$. Following up on the oscillatory behavior, the alignment approaches this field-free value as R increases and the impact of the electric field due to the Rydberg core decreases.

We explore now two sets of electronic states evolving from the Rydberg state $\text{Rb}(23s)$. The adiabatic electronic potentials for $M_J = 0$ and $M_J = 1$ evolving from this Rydberg state and the diatomic molecules in the rotational states with wave functions on the coupled basis Eq. (6) $|N, M_N, 2, 2\rangle$, with $N = 0, 1, 2, 3, 4$, $|3, M_N, 3, 0\rangle$, and $|3, M_N, 0, 3\rangle$, are shown in Fig. 6. All these electronic states approach the same asymptotic limit $\Delta E_{23s} + 12B$ at large separations from the Rydberg core. For $M_J = 0$, there are seven electronic states, and the lowest six are degenerate, forming three pairs [see Fig. 6(a)], whereas for $M_J = 1$, we encounter six states that are pairwise degenerate [see Fig. 6(b)]. The energies of the BOPs evolving from the two KRB molecules in rotational excited states with wave functions $|N, M_N, 3, 3\rangle$, $N = 0, 1, 2, 3, 4, 5, 6$ are shown in Fig. 7; all these electronic states share the asymptotic limit $\Delta E_{23s} + 24B$. There are seven electronic states with $M_J = 0$,

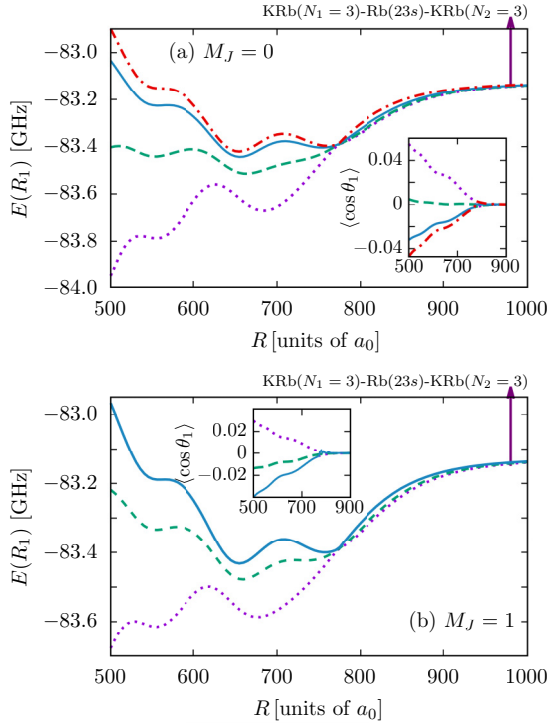


FIG. 7. Symmetric configuration of the Rydberg PentaMol: Adiabatic electronic potential curves ($R = R_1 = R_2$) evolving from the Rydberg state Rb(23s) and the diatomic molecules in rotational excitations $[N, M_N, 3, 3]$ for $N = 0, \dots, 6$. The total magnetic quantum number of the BOPs is (a) $M_J = 0$ and (b) $M_J = 1$. The insets show the orientation of the first diatomic molecule ($\langle \cos \theta_1 \rangle$) located at $\theta_1 = \phi_1 = 0$.

the lowest six forming three pairs of degenerate states, and for $M_J = 1$ there are six states forming three pairs. These BOPs in Figs. 6 and 7 have been computed assuming rotational excitations of the diatomic molecules up to $N_i = 6$, $i = 1, 2$.

These BOPs show an oscillatory behavior with minima reaching depths from a few tenths to a few hundreds of MHz. In these adiabatic electronic states, we encounter unstable configurations of the Rydberg PentaMol with the adiabatic potential energy curves overall decreasing as R decreases and having wells too shallow to accommodate bound vibrational states. For the stable configurations of the Rydberg PentaMol, the BOPs present an asymmetric double-well structure. In the latter potential wells, a few vibrational states exist with vibrational wave functions being delocalized with respect to the two wells. These asymmetric double wells are observed in the two highest-lying electronic states for $M_J = 0$ in Figs. 6(a) and 7(a), and the highest one for $M_J = 1$ in Figs. 6(b) and 7(b).

The energy shifts of these electronic states evolving from Rb(23s) from the corresponding asymptotic limits, i.e., $\Delta E_{23s} + 12B$ and $\Delta E_{23s} + 24B$, are smaller than 2 GHz at $R = 500 a_0$, and are significantly smaller than the shifts of the BOPs from the Rydberg manifold Rb($n = 20$, $l \geq 3$), which reach approximately ~ 45 GHz at $R = 500 a_0$, see Fig. 3. This can be explained in terms of the smaller state space formed by the Rydberg state Rb(23s), which can mix to generate these adiabatic electronic states compared to the large number of Rydberg states with $n = 20$, $l \geq 3$, and m_l forming

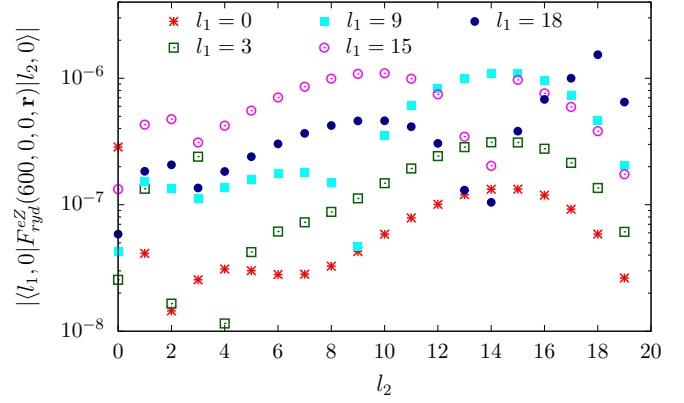


FIG. 8. Matrix elements of the Z component of the electric field due to the Rydberg electron $|\langle l_1, 0 | F_{\text{Ryd}}^{e,Z}(600, 0, 0, \mathbf{r}) | l_2, 0 \rangle|$. See the Appendix for the expression of the Rydberg electron electric field $F_{\text{Ryd}}^{e,Z}(R_i, \theta_i, \phi_i, \mathbf{r})$ in Eqs. (A3) and (A6).

the degenerate manifold Rb($n = 20$, $l \geq 3$), contributing to the BOPs presented in Fig. 3. In addition, the electric fields due to the Rydberg electron of Rb(23s) are weaker than those from the Rydberg manifold Rb($n = 20$, $l \geq 3$). As an example, we present in Fig. 8 the absolute value of the matrix elements of the electric field along the Z axis for a separation between Rb⁺ and each KRb of $R = 600 a_0$. These matrix elements are defined in the Appendix. Due to the larger spatial extension of the radial wave function of the Rydberg state Rb(23s) compared to those from Rb($n = 20$, $l \geq 3$), the matrix elements $\langle 0, 0 | F_{\text{Ryd}}^{e,Z}(R, 0, 0, \mathbf{r}) | l_2, 0 \rangle$ with $l_2 \geq 3$ are in most cases smaller than those involving two wave functions of the degenerate manifold. In addition, within the degenerate manifold there are many nonzero matrix elements of the electric-field components, $\langle l_1, m_1 | F_{\text{Ryd}}^{e,Z}(R, 0, 0, \mathbf{r}) | l_2, m_2 \rangle$, $l_1, l_2 \geq 3$, affecting the two diatomic molecules, compared to the few nonzero components due to the coupling of Rb(23s) with the Rb($n = 20$, $l \geq 3$) states, i.e., $\langle 0, 0 | F_{\text{Ryd}}^{e,Z}(R, 0, 0, \mathbf{r}) | l_j, 0 \rangle$ and $\langle 0, 0 | F_{\text{Ryd}}^{e,Z}(R, 0, 0, \mathbf{r}) | l_j, \pm 1 \rangle$. Since the interaction with the electric field produces the same impact on both diatomic molecules, the BOPs become degenerate.

Regarding the directional properties of the KRb molecules, we present only the orientation of the first diatomic molecule, since for the orientation of the second one, it holds $\langle \cos \theta_2 \rangle = -\langle \cos \theta_1 \rangle$. As can be observed in the insets of Figs. 6 and 7, the orientation is very small due to the weak electric fields created by the Rydberg electron in Rb(23s). Additionally, the large rotational excitations give rise to large kinetic energies, which should be compensated by the interaction with the Rydberg electric field. In contrast, for the two diatomic molecules within the lowest-lying potential evolving from Rb(23s), i.e., the KRb molecules in $N_1 = N_2 = 0$, not shown here, we obtain $|\langle \cos \theta_i \rangle| = 0.32$ for $R = 500 a_0$, which is similar to the orientation achieved for the lowest-lying BOP from the degenerate manifold presented in Fig. 5(a).

B. The linear asymmetric Rydberg molecule

Next we explore the electronic structure of the Rydberg PentaMol in two asymmetric configurations with the two

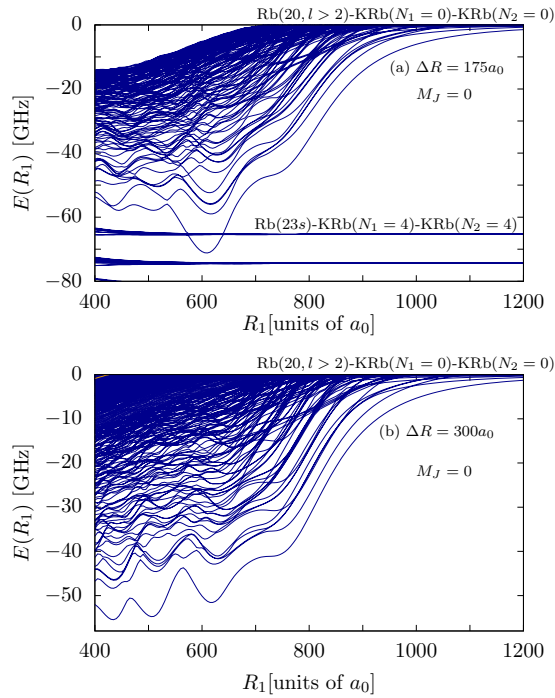


FIG. 9. Asymmetric Rydberg PentaMol: Adiabatic electronic potentials evolving from the Rydberg manifold $\text{Rb}(n = 20, l \geq 3)$ versus the separation of the first dipole R_1 from Rb^+ . The second diatomic molecule is located at the same side of the Rb^+ core and separated from the first one by a distance (a) $\Delta R = 175 a_0$ and (b) $\Delta R = 300 a_0$, which is kept constant. The first (1) and second (2) KRb molecules are shown in the sketch of Fig. 1(b).

diatomic molecules located at the same side of the Rydberg core Rb-KRb-KRb , e.g., Fig. 1(b). The calculations have been done using rotational excitations of KRb up to $N_i = 4, i = 1, 2$. The separation between the two diatomic molecules is kept large enough so that the dipole-dipole interaction between the molecules is neglected. For instance, this dipole-dipole interaction amounts to approximately 0.11 GHz for two fully oriented KRb molecules separated by $150 a_0$, which is significantly smaller than the few tens of GHz energy shifts from the Rydberg manifold obtained for both the symmetric and asymmetric configurations of the ultralong-range Rydberg PentaMol.

First, we consider the Rydberg PentaMol in which the distances of the two KRb molecules from the Rydberg core increase, while their relative separation is kept constant with example values $\Delta R = R_2 - R_1 = 175 a_0$ and $300 a_0$. The adiabatic potential curves for $M_J = 0$ are shown in Fig. 9 as a function of the distance of the first diatomic molecule R_1 from Rb^+ . The lowest-lying BOP from this Rydberg manifold is energetically well separated from the other electronic BOPs. Compared to the Rydberg TriMol and to the symmetric configuration of KRb-Rb-KRb , the energy shifts of the adiabatic potentials from the Rydberg manifold $\text{Rb}(n = 20, l \geq 3)$ are larger. The wells of these BOPs possess depths of a few GHz, and we estimate that a few tens of vibrational bound states should exist in the outermost potential well. For the asymmetric linear configuration, the two diatomic molecules are exposed to electric fields of different strengths

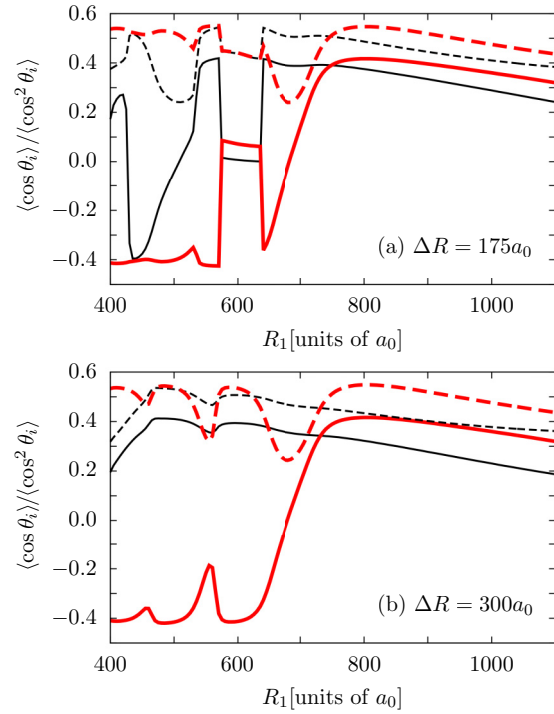


FIG. 10. Orientation (solid lines) and alignment (dashed lines) of the first (thick red lines) and second (thin black lines) diatomic molecules within the lowest-lying BOP for $M_J = 0$ evolving from the Rydberg manifold $\text{Rb}(n = 20, l \geq 3)$ for the Rydberg PentaMol in an asymmetric configuration as a function of R_1 . The relative separation between the two diatomic molecules is kept fixed to (a) $\Delta R = 175 a_0$ and (b) $\Delta R = 300 a_0$, and they are both located on the same side of the Rb^+ core. The first (1) and second (2) KRb molecules are shown in the sketch of Fig. 1(b).

but along the same direction. As a consequence, the effect of the Rydberg field on the two diatomic molecules becomes additive, and the energy shifts become larger than for the symmetric Rydberg molecule. For $\Delta R = 175 a_0$ in Fig. 9(a), the minimum of the lowest-lying adiabatic potential is below the BOP evolving from $\text{Rb}(23s)$, the diatomic molecules being in the rotational excitations $|N, M_N, 4, 4\rangle$, and these two sets of adiabatic electronic states exhibit several avoided crossings.

Let us now analyze the directional properties of the KRb molecules in this asymmetric configuration of the Rydberg molecule Fig. 10. For $\Delta R = 300 a_0$ in Fig. 10(b), the first diatomic molecule shows a similar orientation and alignment as in the symmetric configuration. The second KRb is located $300 a_0$ further away from the Rb^+ than the first one; as a consequence, it is oriented oppositely with respect to the Rydberg core, and after an oscillation its value monotonically decreases. For $\Delta R = 175 a_0$ in Fig. 10(a), the orientation and alignment of the two KRb show a more complex behavior as R_1 increases, which is characterized by sudden changes for $R_1 \approx 580 a_0$ and $R_1 \approx 640 a_0$, due to the avoided crossings with the BOPs evolving from the Rydberg state $\text{Rb}(23s)$ and the diatomic molecules in the rotational excitations $|N, M_N, 4, 4\rangle$. Between these two values of R_1 , the alignment and orientation keep an almost constant value. For $R_1 \gtrsim 640 a_0$, the orientation and alignment behavior of the two diatomic molecule resemble

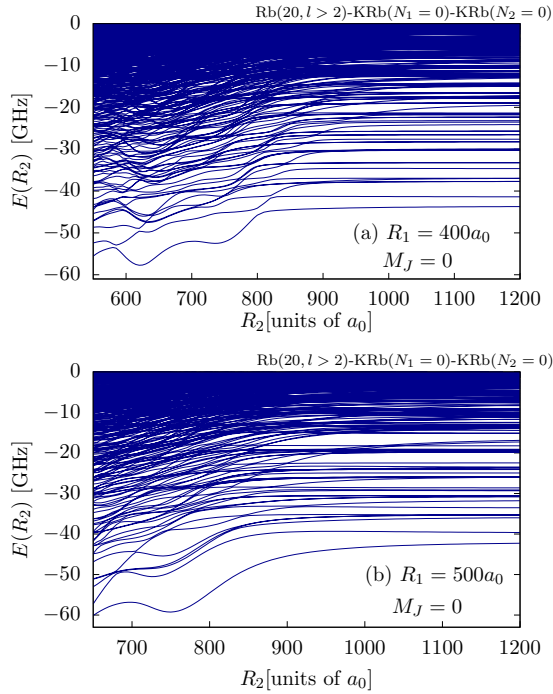


FIG. 11. Asymmetric Rydberg PentaMol: Adiabatic electronic potentials evolving from the Rydberg manifold $\text{Rb}(n = 20, l \geq 3)$ versus the separation of the second diatomic molecule R_2 from Rb^+ . The position of the first diatomic molecule is fixed at (a) $R_1 = 400 a_0$ and (b) $R_1 = 500 a_0$. Both diatomic molecules are located at the same side of the Rb^+ core, see Fig. 1(b).

those from the configuration with the relative separation $\Delta R = 300 a_0$, monotonically decreasing and approaching the corresponding field-free values 0 and $1/3$, respectively, in the limit of very large separations between the two diatomic molecules and the Rydberg core.

In the second asymmetric configuration, we assume that the position of the first diatomic molecule is fixed, whereas the separation of the second one from the Rydberg core R_2 increases. The corresponding BOPs when the first KRb molecule is located at $R_1 = 400 a_0$ and $R_1 = 500 a_0$ are presented in Figs. 11(a) and 11(b), respectively. As for the previous asymmetric configuration, the energy shifts are also larger here when compared to the symmetric configuration of the Rydberg PentaMol, which is due to the additive effect of the Rydberg electric fields in both diatomic molecules. The lowest-lying potentials from the Rydberg manifold $\text{Rb}(n = 20, l \geq 3)$ present an oscillatory behavior with broad minima of a few GHz depths. For the asymmetric configuration with the first KRb located at $R_1 = 400 a_0$, the outermost minimum of this energetically lowest-lying BOP is too shallow to accommodate vibrational bound states. In the first minimum of this BOP located at around $R_2 \approx 622 a_0$ [see Fig. 11(a)], we estimate approximately six vibrational bound states. If the first KRb is located at $R_1 = 500 a_0$, there are also a few bound vibrational states in the outermost minimum. From there on, they reach a plateaulike behavior for large values of R_2 . In this limit, the BOPs approach the energies of the Rydberg TriMol with the KRb located either at $R_1 = 400 a_0$ or $R_1 = 500 a_0$ [see Figs. 11(a) and 11(b)].

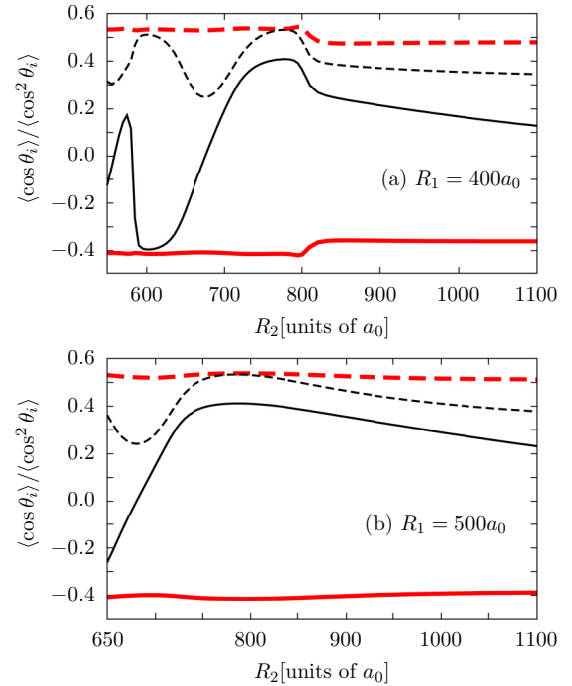


FIG. 12. Orientation (solid lines) and alignment (dashed lines) of the first (thick red lines) and second (thin black lines) diatomic molecules within the lowest-lying BOP for $M_J = 0$ evolving from the Rydberg manifold $\text{Rb}(n = 20, l \geq 3)$ in the Rydberg PentaMol in an asymmetric configuration where the position of the first diatomic molecule is fixed on (a) $R_1 = 400 a_0$ and (b) $R_1 = 500 a_0$. Both diatomic molecules are located at the same side of the Rb^+ core. The first (1) and second (2) KRb molecules are shown in the sketch of Fig. 1(b).

Finally, we analyze the rotational dynamics of the two diatomic molecules in the Rydberg PentaMol in this second asymmetric configuration in Figs. 12(a) and 12(b) when the position of the first diatomic molecule is fixed at $R_1 = 400 a_0$ and $R_1 = 500 a_0$, respectively. For both values of R_1 , the first diatomic molecule is moderately antioriented and aligned, and both expectation values present a plateaulike behavior as R_2 increases. In contrast, the directional properties of the second KRb oscillate as R_2 increases [see Figs. 12(a) and 12(b)]; it is first antioriented and becomes oriented once the interaction due to the Rydberg core electric field starts to dominate. For large values of R_2 , the orientation and alignment of this second diatomic molecule approach the field-free values 0 and $1/3$, respectively.

IV. CONCLUSIONS

We have investigated ultralong-range Rydberg penta-atomic molecules formed by a Rydberg rubidium atom and two KRb diatomic rotational molecules. The binding mechanism of these exotic molecules is due to the interaction of the electric dipole moments of the diatomic molecules with the electric fields due to the Rydberg electron and Rydberg core. Within the rigid rotor approximation, we have taken into account the rotational motion of the diatomic molecules, providing a proper description of the hybridization of their

rotational motion due to the Rydberg electric fields. For the considered configurations of the penta-atomic molecule, we can neglect the dipole-dipole interaction between the two diatomic molecules, which is a couple of orders of magnitude smaller than the transition frequencies.

The Born-Oppenheimer potential curves for $M_J = 0, 1$ for the Rydberg penta-atomic molecule as a function of the separations between the Rb^+ core and the KRb molecules have been obtained and analyzed. The structures of these BOPs strongly depend on the Rydberg state of Rb forming the corresponding electronic state. For the linear symmetric and asymmetric configurations, these results demonstrate that the Rydberg penta-atomic molecule could exist in stable adiabatic electronic states evolving from the degenerate manifold $\text{Rb}(n = 20, l \geq 3)$, which possess potential wells with depths of a few GHz. Involving the $\text{Rb}(23s)$ state, we encounter unstable electronic states but also stable ones possessing potential wells with depths of a few hundred MHz. For these electronic states evolving either from $\text{Rb}(n = 20, l \geq 3)$ or $\text{Rb}(23s)$, the corresponding potential wells can accommodate a few vibrational bound levels where the Rydberg penta-atomic molecules exist. In addition, we have studied the directional properties, i.e., orientation and alignment, of the two KRb molecules within the Rydberg penta-atomic molecule. The diatomic molecules show a significant orientation and alignment in the BOPs evolving from the Rydberg degenerate manifold. In contrast, these molecules exhibit minor orientation for the electronic states $\text{Rb}(23s)$ together with the KRb molecules being in excited rotational states.

A natural extension of this work would be to investigate these Rydberg penta-atomic molecules in a planar triangular configuration to describe the system formed by the two diatomic molecules located at the minima of an optical lattice and the Rydberg atom above them. In such a configuration, the azimuthal symmetry is lost and the total magnetic quantum number is not conserved. Thus, the basis set expansion of the wave function should include the coupled wave functions (5) with all possible values of M_J , i.e., $|M_J| \leq J$. As a consequence, the size of the Hamiltonian matrix becomes very large, being computationally very challenging to obtain the eigenvalues. For instance, including the Rydberg manifold $\text{Rb}(n = 20, l \geq 3)$ and $\text{Rb}(23s)$, and rotational excitations up to $N_i = 5$, the dimension of the Hamiltonian matrix is larger than half a million when the Rydberg penta-atomic molecule has this triangular configuration. One could also

consider more complex ultralong-range Rydberg molecules formed by one Rydberg atom and several diatomic polar molecules in different configurations. Such systems could be explored by considering diatomic open-shell diatomic molecules such as OH , OD , LiO , and NaO , whose rotational spectra in external fields are characterized by fine-structure interactions and the Λ -doubling effects [40]. For sufficiently weak electric fields, the rotational motion of these molecules could be described using a two-state model [41,42], which facilitates their computational analysis and renders it realistic to obtain the adiabatic electronic potential curves and surfaces of the polyatomic ultralong-range Rydberg molecules as it was previously done for the triatomic Rydberg molecule [23–25].

ACKNOWLEDGMENTS

R.G.F. and J.A.F. acknowledge financial support by the Spanish MINECO through Project No. FIS2014-54497-P and the Andalusian research group FQM-207. P.S. acknowledges financial support by the Deutsche Forschungsgemeinschaft (DFG) in the framework of the Schwerpunktprogramm SPP 1929 “Giant Interactions in Rydberg System.” R.G.F. and P.S. acknowledge the hospitality of the Kavli Institute for Theoretical Physics at the University of California Santa Barbara in the framework of the workshop “Universality in Few-Body Systems.” This research was supported in part by the National Science Foundation under Grant No. NSF PHY11-25915. R.G.F. and P.S. acknowledge the Institute for Theoretical Atomic, Molecular and Optical Physics (ITAMP) at the Harvard-Smithsonian Center for Astrophysics for support. H.R.S. was supported through a grant from the NSF to ITAMP.

APPENDIX: THE RYDBERG ELECTRON ELECTRIC FIELD

In this Appendix we provide the expression of the electric field created by the Rydberg electron at the positions of the diatomic molecules which are in Cartesian coordinates given by

$$\mathbf{F}_{\text{Ryd}}^e(\mathbf{R}_i, \mathbf{r}) = e \frac{\mathbf{r} - \mathbf{R}_i}{|\mathbf{r} - \mathbf{R}_i|^3} = \nabla_{\mathbf{R}_i} \frac{1}{|\mathbf{r} - \mathbf{R}_i|}, \quad (\text{A1})$$

where $\nabla_{\mathbf{R}_i}$ is the Laplacian with respect to the molecular coordinate \mathbf{R}_i with $i = 1, 2$, see Ref. [43]. The electric field reads

$$\mathbf{F}_{\text{Ryd}}^e(R_i, \Omega_i, \mathbf{r}) = F_{\text{Ryd}}^{e,X}(R_i, \Omega_i, \mathbf{r})\hat{X} + F_{\text{Ryd}}^{e,Y}(R_i, \Omega_i, \mathbf{r})\hat{Y} + F_{\text{Ryd}}^{e,Z}(R_i, \Omega_i, \mathbf{r})\hat{Z}, \quad (\text{A2})$$

$$F_{\text{Ryd}}^{e,K}(R_i, \Omega_i, \mathbf{r}) = e \sum_{l=0}^{\infty} \frac{4\pi}{2l+1} \begin{cases} -(l+1) \frac{r^l}{R_i^{l+2}} \sum_{m=-l}^l Y_{lm}(\Omega) A_{lm}^K(\Omega_i) \hat{K} & \text{if } r < R_i \\ l \frac{R_i^{l-1}}{r^{l+1}} \sum_{m=-l}^l Y_{lm}(\Omega) A_{lm}^K(\Omega_i) \hat{K} & \text{if } r > R_i, \end{cases} \quad (\text{A3})$$

with $K = X, Y$, and Z . The coordinates of the Rydberg electron are \mathbf{r} and $\Omega = (\theta, \phi)$, whereas (R_i, θ_i, ϕ_i) are the coordinates of the center of mass of the i th diatomic molecule for $i = 1, 2$, with $\Omega_i = (\theta_i, \phi_i)$ being the Euler angles. The components $A_{lm}^K(\Omega_i)$ read

$$A_{lm}^X(\Omega_i) = [Y_{lm}^*(\Omega_i) \sin \theta_i \cos \phi_i + (Y_{lm+1}^*(\Omega_i) e^{i\phi_i} a_{lm} - Y_{lm-1}^*(\Omega_i) e^{-i\phi_i} b_{lm}) \cos \theta_i \cos \phi_i - i(Y_{lm+1}^*(\Omega_i) e^{-i\phi_i} a_{lm} + Y_{lm-1}^*(\Omega_i) e^{i\phi_i} b_{lm}) \sin \theta_i], \quad (\text{A4})$$

$$A_{lm}^Y(\Omega_i) = [Y_{lm}^*(\Omega_i) \sin \theta_i \sin \phi_i + (Y_{lm+1}^*(\Omega_i)e^{i\phi_i}a_{lm} - Y_{lm-1}^*(\Omega_i)e^{-i\phi_i}b_{lm}) \cos \theta_i \sin \phi_i + i(Y_{lm+1}^*(\Omega_i)e^{-i\phi_i}a_{lm} + Y_{lm-1}^*(\Omega_i)e^{+i\phi_i}b_{lm}) \cos \theta_i], \quad (\text{A5})$$

$$A_{lm}^Z(\Omega_i) = [Y_{lm}^*(\Omega_i) \cos \theta_i - (Y_{lm+1}^*(\Omega_i)e^{i\phi_i}a_{lm} - Y_{lm-1}^*(\Omega_i)e^{-i\phi_i}b_{lm}) \sin \theta_i], \quad (\text{A6})$$

with

$$a_{lm} = \sqrt{l(l+1) - m(m+1)}, \quad (\text{A7})$$

$$b_{lm} = \sqrt{l(l+1) - m(m-1)}. \quad (\text{A8})$$

If the two diatomic molecules are located along the Z axis, the expression for the electric field is significantly simplified because $\theta_i = 0$ or $\theta_i = \pi$, and $\phi_i = 0$. For $\theta_i = 0$ and $\phi_i = 0$, we obtain

$$A_{lm}^X(0,0) = \sqrt{\frac{2l+1}{4\pi}}(\delta_{m,-1}a_{lm} - \delta_{m,1}b_{lm}), \quad (\text{A9})$$

$$A_{lm}^Y(0,0) = -i\sqrt{\frac{2l+1}{4\pi}}(\delta_{m,-1}a_{lm} + \delta_{m,1}b_{lm}), \quad (\text{A10})$$

$$A_{lm}^Z(0,0) = \sqrt{\frac{2l+1}{4\pi}}\delta_{m,0}, \quad (\text{A11})$$

where δ_{m_1, m_2} is the Kronecker δ . If the diatomic molecule is located at the other side of the Rydberg core, $\theta_i = \pi$ and $\phi_i = 0$, we obtain

$$A_{lm}^X(\pi,0) = (-1)^{l+1}\sqrt{\frac{2l+1}{4\pi}}(\delta_{m,-1}a_{lm} - \delta_{m,1}b_{lm}), \quad (\text{A12})$$

$$A_{lm}^Y(\pi,0) = i(-1)^l\sqrt{\frac{2l+1}{4\pi}}(\delta_{m,-1}a_{lm} + \delta_{m,1}b_{lm}), \quad (\text{A13})$$

$$A_{lm}^Z(\pi,0) = (-1)^{l+1}\sqrt{\frac{2l+1}{4\pi}}\delta_{m,0}. \quad (\text{A14})$$

For the Z component of $\mathbf{F}_{\text{Ryd}}^e(\mathbf{R}_i, \mathbf{r})$ in Eq. (A3), the sum in the magnetic quantum number m is restricted to $m = 0$, whereas for the X and Y components, only the terms with $m = 1$ and -1 contribute.

For the symmetric configuration, i.e., the two diatomic molecules are located at different sides of the Rb^+ core and $R_1 = R_2$, the l -dependent components of the electric field are of the same strength but differ with respect to the sign, depending on the orbital angular momentum of the Rydberg electron l . As a consequence, the matrix elements of the electric-field components satisfy the following relation:

$$\langle l_1, m_1 | F_{\text{Ryd}}^{e,K}(R_1, 0, 0, \mathbf{r}) | l_2, m_2 \rangle = -(-1)^{l_1 - l_2} \langle l_1, m_1 | F_{\text{Ryd}}^{e,K}(R_2, \pi, 0, \mathbf{r}) | l_2, m_2 \rangle, \quad (\text{A15})$$

with $K = X, Y, Z$ and $R_1 = R_2$. The matrix element of the Z component of the electric field is nonzero if $m_1 = m_2$, whereas nonzero contributions of the electric field along the X and Y axes are obtained if $m_2 = m_1 \pm 1$. In addition, the following relations between the electric-field components along the X and Y axes are satisfied:

$$\langle l_1, m_1 | F_{\text{Ryd}}^{e,X}(R_i, \theta_i, 0, \mathbf{r}) | l_2, m_1 + 1 \rangle = i \langle l_1, m_1 | F_{\text{Ryd}}^{e,Y}(R_i, \theta_i, 0, \mathbf{r}) | l_2, m_1 + 1 \rangle, \quad (\text{A16})$$

$$\langle l_1, m_1 | F_{\text{Ryd}}^{e,X}(R_i, \theta_i, 0, \mathbf{r}) | l_2, m_1 - 1 \rangle = -i \langle l_1, m_1 | F_{\text{Ryd}}^{e,Y}(R_i, \theta_i, 0, \mathbf{r}) | l_2, m_1 - 1 \rangle, \quad (\text{A17})$$

with $i = 1, 2$ and $\theta_1 = 0$ and $\theta_2 = \pi$. Note that although the electric-field component along the Y axis is imaginary, the Hamiltonian matrix is real because the matrix elements of the electric dipole moment of the diatomic molecules along the Y -axis laboratory fixed frame is also imaginary.

-
- [1] A. Krüchow, A. Mohammadi, A. Härter, and J. Hecker Denschlag, *Phys. Rev. A* **94**, 030701(R) (2016).
[2] S. Kotler, R. W. Simmonds, D. Leibfried, and D. J. Wineland, *Phys. Rev. A* **95**, 022327 (2017).
[3] M. Gröbner, P. Weinmann, F. Meinert, K. Lauber, E. Kirilov, and H.-C. Nägerl, *J. Mod. Opt.* **63**, 1829 (2016).

- [4] R. Côté, V. Kharchenko, and M. D. Lukin, *Phys. Rev. Lett.* **89**, 093001 (2002).
[5] F. H. J. Hall and S. Willitsch, *Phys. Rev. Lett.* **109**, 233202 (2012).
[6] M. Schlagmüller, T. C. Liebisch, F. Engel, K. S. Kleinbach, F. Böttcher, U. Hermann, K. M. Westphal, A. Gaj, R. Löw,

- S. Hofferberth, T. Pfau, J. Pérez-Ríos, and C. H. Greene, *Phys. Rev. X* **6**, 031020 (2016).
- [7] T. Secker, R. Gerritsma, A. W. Glaetzle, and A. Negretti, *Phys. Rev. A* **94**, 013420 (2016).
- [8] P. Eberle, A. D. Dörfler, C. von Planta, K. Ravi, and S. Willitsch, *Chem. Phys. Chem.* **17**, 3769 (2016).
- [9] S. Ospelkaus, K.-K. Ni, D. Wang, M. H. G. De Miranda, B. Neyenhuis, G. Quémener, P. S. Julienne, J. L. Bohn, D. S. Jin, and J. Ye, *Science* **327**, 853 (2010).
- [10] G. Kurizki, P. Bertet, Y. Kubo, K. Mølmer, D. Petrosyan, P. Rabl, and J. Schmiedmayer, *Proc. Natl. Acad. Sci. U.S.A.* **112**, 3866 (2015).
- [11] C. H. Greene, A. S. Dickinson, and H. R. Sadeghpour, *Phys. Rev. Lett.* **85**, 2458 (2000).
- [12] E. Fermi, *Nuovo Cimento* **11**, 157 (1934).
- [13] A. Omont, *J. Phys.* **38**, 1343 (1977).
- [14] V. Bendkowsky, B. Butscher, J. Nipper, J. P. Shaffer, R. Löw, and T. Pfau, *Nature (London)* **458**, 1005 (2009).
- [15] M. A. Bellos, R. Carollo, J. Banerjee, E. E. Eyler, P. L. Gould, and W. C. Stwalley, *Phys. Rev. Lett.* **111**, 053001 (2013).
- [16] D. A. Anderson, S. A. Miller, and G. Raithel, *Phys. Rev. Lett.* **112**, 163201 (2014).
- [17] A. T. Krupp, A. Gaj, J. B. Balewski, P. Ilzhöfer, S. Hofferberth, R. Löw, T. Pfau, M. Kurz, and P. Schmelcher, *Phys. Rev. Lett.* **112**, 143008 (2014).
- [18] H. Saßmannshausen, F. Merkt, and J. Deiglmayr, *Phys. Rev. Lett.* **114**, 133201 (2015).
- [19] D. Booth, S. T. Rittenhouse, J. Yang, H. R. Sadeghpour, and J. P. Shaffer, *Science* **348**, 99 (2015).
- [20] T. Niederprüm, O. Thomas, T. Eichert, C. Lippe, J. Pérez-Ríos, C. H. Greene, and H. Ott, *Nat. Commun.* **7**, 12820 (2016).
- [21] F. Camargo, J. D. Whalen, R. Ding, H. R. Sadeghpour, S. Yoshida, J. Burgdörfer, F. B. Dunning, and T. C. Killian, *Phys. Rev. A* **93**, 022702 (2016).
- [22] J. D. Whalen, F. J. D. Whalen, F. Camargo, R. Ding, T. C. Killian, F. B. Dunning, J. Pérez-Ríos, S. Yoshida, and J. Burgdörfer, *Phys. Rev. A* **96**, 042702 (2017).
- [23] S. T. Rittenhouse and H. R. Sadeghpour, *Phys. Rev. Lett.* **104**, 243002 (2010).
- [24] S. T. Rittenhouse, M. Mayle, P. Schmelcher, and H. R. Sadeghpour, *J. Phys. B* **44**, 184005 (2011).
- [25] M. Mayle, S. T. Rittenhouse, P. Schmelcher, and H. R. Sadeghpour, *Phys. Rev. A* **85**, 052511 (2012).
- [26] R. González-Férez, H. R. Sadeghpour, and P. Schmelcher, *New J. Phys.* **17**, 013021 (2015).
- [27] E. Fermi and E. Teller, *Phys. Rev.* **72**, 399 (1947).
- [28] J. E. Turner, *Am. J. Phys.* **45**, 758 (1977).
- [29] C. W. Clark, *Phys. Rev. A* **20**, 1875 (1979).
- [30] H. Hotop, M.-W. Rul, and I. I. Fabrikant, *Phys. Scr.* **2004**, 22 (2004).
- [31] J. Aguilera-Fernández, H. R. Sadeghpour, P. Schmelcher, and R. González-Férez, *J. Phys.: Conf. Ser.* **635**, 012023 (2015).
- [32] E. Kuznetsova, R. Côté, K. Kirby, and S. F. Yelin, *Phys. Rev. A* **78**, 012313 (2008).
- [33] E. Kuznetsova, S. T. Rittenhouse, H. R. Sadeghpour, and S. F. Yelin, *Phys. Rev. A* **94**, 032325 (2016).
- [34] M. Zeppenfeld, *Europhys. Lett.* **118**, 13002 (2017).
- [35] K.-K. Ni, S. Ospelkaus, D. J. Nesbitt, J. Ye, and D. S. Jin, *Phys. Chem. Chem. Phys.* **11**, 9626 (2009).
- [36] K.-K. Ni, S. Ospelkaus, M. H. G. de Miranda, A. Pe'er, B. Neyenhuis, J. J. Zirbel, S. Kotochigova, P. S. Julienne, D. S. Jin, and J. Ye, *Science* **322**, 231 (2008).
- [37] R. González-Férez and P. Schmelcher, *Phys. Rev. A* **69**, 023402 (2004).
- [38] R. González-Férez and P. Schmelcher, *Phys. Rev. A* **71**, 033416 (2005).
- [39] M. Marinescu, H. R. Sadeghpour, and A. Dalgarno, *Phys. Rev. A* **49**, 982 (1994).
- [40] M. Gärtner, J. J. Omiste, P. Schmelcher, and R. González-Férez, *Mol. Phys.* **111**, 1865 (2013).
- [41] M. Lara, B. L. Lev, and J. L. Bohn, *Phys. Rev. A* **78**, 033433 (2008).
- [42] B. K. Stuhl, M. Yeo, B. C. Sawyer, M. T. Hummon, and J. Ye, *Phys. Rev. A* **85**, 033427 (2012).
- [43] K. Ayuel and P. de Chatel, *Physica B* **404**, 1209 (2009).